Materials Horizons

ROYAL SOCIETY OF CHEMISTRY

COMMUNICATION

View Article Online
View Journal | View Issue

Check for updates

Cite this: *Mater. Horiz.*, 2024, 11, 5114

Received 15th May 2024,
Accepted 30th July 2024

DOI: 10.1039/d4mh00591k

rsc.li/materials-horizons

Published on 01 August 2024. Downloaded on 9/9/2025 11:02:34 PM.

A lignin-derived carbon dot-upgraded bacterial cellulose membrane as an all-in-one interfacial evaporator for solar-driven water purification†

Nirmiti Mate,[a] Kallayi Nabeela,[b] Gopika Preethikumar,[cd] Saju Pillai *[cd] and Shaikh M. Mobin *[ab]

Solar-driven interfacial evaporation has emerged as an efficient approach for wastewater treatment and seawater desalination. New trends demand adaptive technology to develop photothermal membranes with multifunctional features. Herein, we report a robust multi-purpose near-infrared (NIR)-active hydrogel composite (*c*-BC@N-LCD) from broad-spectrum active nitrogen-doped lignin-derived carbon dots (N-LCDs) covalently cross-linked with a bacterial cellulose (BC) matrix. BC provides adequate porosity and hydrophilicity required for easy water transport while managing heat loss. A commendable evaporation rate (ER) of 2.2 kg m^{-2} h^{-1} under one sun (1 kW m^{-2}) is achieved by *c*-BC@N-LCD. The developed hydrogel system is also found to be efficient for desalination (~2.1 kg m^{-2} h^{-1}) and for remediating various pollutants (heavy metal ions, dyes, and pharmaceuticals) from feed water. The efficacy of the membrane remains unaltered by different grades of water, and hence can be adoptable for economically stressed communities living in water-polluted regions as well as those residing in coastal areas.

New concepts

Developing advanced water treatment technologies with an environmentally benign strategy is very important for addressing the water scarcity and environmental crisis. Carbon dots (CDs) are one of the emerging classes of nanomaterial that has been explored as a photothermal material due to their broadband absorption, biocompatibility, stability, and scalability. In this work, N-doped lignin-derived carbon dots (N-LCDs) as a broad-spectrum active photothermal material are stabilized on a bacteria-biosynthesized nanocellulose membrane, *i.e.* bacterial cellulose (BC), by covalent cross-linking (*c*-BC@N-LCD) without compromising their photocatalytic activity. For the first time, an adaptive single-step one-pot synthesis route has been applied for fabricating an all-in-one interfacial evaporator applicable for both solar freshwater production and water pollutant remediation. The designed *c*-BC@N-LCD achieve a distinguished evaporation rate of 2.2 kg m^{-2} h^{-1} under one sun (1 kW m^{-2}). Furthermore, the developed hydrogel system has also been found to be efficient for desalination (~2.1 kg m^{-2} h^{-1}) and for remediating various pollutants (heavy metal ions, dyes, and pharmaceuticals) from feed water. Altogether, the present *c*-BC@N-LCD hydrogel acts as a multifunctional evaporator that is durable, reusable, and robust even after multiple purification cycles and having a wide range of applications, ranging from large-scale industrial platforms to eco-friendly portable water purifying appliances.

Introduction

Freshwater scarcity is one of the greatest global problems due to water pollution, over-exploitation of water resources, and natural calamities in some underdeveloped and developing countries.[1,2] Currently, the water purification, desalination, and remediation systems are not economically viable since they involve inefficient energy utilization and sophisticated infrastructure.[3,4] Many efforts have been made to develop more economical, environmentally friendly, and convenient technologies for solar clean water production.[5,6] One such technique involves the utilization of solar energy. Solar energy is the most abundant green alternative to fossil fuels that one can exploit for freshwater production.[7,8] Currently, solar desalination through interfacial evaporation is the most energy efficient strategy for the production of freshwater.[9]

In this respect, water technology has been reinforced by a variety of interfacial solar evaporator designs, which have attracted attention in recent years. A solar evaporator absorbs the solar energy through a photothermally active material and generates heat at the water–air interface and converts water

[a] *Department of Chemistry, Indian Institute of Technology Indore, Simrol, Khandwa Road, Indore 453552, India*
[b] *Centre for Advanced Electronics (CAE), Indian Institute of Technology (IIT) Indore, Simrol, Khandwa Road, Indore 453552, India*
[c] *Materials Science and Technology Division, CSIR-National Institute for Interdisciplinary Science and Technology (NIIST), Thiruvananthapuram, Kerala 695 019, India*
[d] *Materials Science and Technology Division, CSIR-National Institute for Interdisciplinary Science and Technology (NIIST), Thiruvananthapuram, Kerala 695 019, India. E-mail: xray@iiti.ac.in*

† Electronic supplementary information (ESI) available. See DOI: https://doi.org/10.1039/d4mh00591k

This journal is © The Royal Society of Chemistry 2024

Published on 01 August 2024. Downloaded on 9/9/2025 11:02:34 PM.

into steam to obtain clean water.[10–12] Highly efficient, wide-range absorption and excellent light to heat converting materials are perquisites for solar steam generation.[13,14] Previously, many photothermal materials have been exploited for photothermal conversion, such as carbonaceous materials,[15] graphene,[16,17] CNTs,[18,19] plasmonic structures,[20] polymers,[21] semiconductors,[22,23] metal organic frameworks,[24] *etc.* Most such materials have limited applicability due to their high fabrication cost, tedious synthesis, non-environmentally friendly nature and insufficient scalability.

Interestingly, carbon-based quantum dots (CDs) are one of the emerging classes of nanomaterials with excellent broadband absorption (in near-infrared (NIR) range) with interesting optical properties, and distinct applicability.[25,26] Most importantly, CDs are environmentally friendly and can be easily synthesized from simple or complex organic materials. Recently, plant-derived organic compounds have been utilized as a green source[27] to attribute improved photophysical properties and biocompatibility to CDs.[28] Being the second largest naturally occurring organic material on earth, lignin has also been explored as a green precursor for synthesizing CDs. Unlike cellulose, lignin has three dimensional and cross-linked phenolic networks, possessing high carbon content by virtue of the large proportion of sp^2 hybridised benzene rings. These features together with abundant phenolic –OH groups promote the formation of CDs.[29] Furthermore, lignin can be derived from renewable sources, which primarily exist as a waste by-product from the paper-pulp industry.[30]

Moreover, the photophysical properties of CDs have also been explored for the degradation of organic pollutants by utilizing the entire solar spectrum by electron–hole recombination and enhancing the photocatalytic degradation.[31] Furthermore, tunable photophysical properties of CDs can also be constructively exploited for solar thermal evaporation. The high solar light absorption, stability and scalability of CDs are beneficial for such application. CDs have graphite-like sp^2 carbon clusters,[32] which enable them to show lattice vibration when irradiated with solar light and convert it into thermal energy. During the electron transition of CDs after absorbing the energy, it undergoes an energy level transition as well as nonradiative transitions, and such transition allows the CDs to release some energy in the form of heat. This thermal energy can further be utilized for photothermal water evaporation.[33]

However, the only hurdle in the case of CDs is their tiny size (>10 nm), rendering slow leaching in water media. Therefore, achieving better recyclability demands appending this material onto some polymeric porous matrix. Previously, CDs have been incorporated into porous matrices to form composite materials that can be used for drug delivery,[34] light-emitting devices,[35] sensing,[36] energy applications,[37] photodynamic therapy,[38] *etc.* As for steam generation application, polymeric hydrogels enable the integration of nanostructured CDs into macroscopic materials.[39–41] The assembled composite hydrogels have novel properties, utilized in practical applications such as waste water treatment,[42] catalysis,[43] *etc.* In this regard, bacterial cellulose (BC), having a highly porous nanofibrous network structure, was explored due to its strong mechanical properties, flexibility, biocompatibility, and thermal stability. BC on the other hand is a green alternative to artificial polymers[44] that are currently been explored for such applications. The porosity and hydrophilicity of BC, which promote water transport and lower thermal conductivity, cause less heat loss to the bulk water during solar evaporation.[45] Several groups have explored the potential of BC as a solar evaporating platform hybridized with photothermally active material for solar evaporation processes.[45–47]

In recent times, researchers have integrated multiple methods and exploited different properties of photothermal evaporator materials. For instance, Song *et al.* developed a polyamide thin film membrane for forward osmosis and a polypyrrole-modified nanosponge for photothermal evaporation. This coupling system comprehensively utilized the advantages of both techniques, which improves the separation efficiency for wastewater treatment.[48] Similarly, various carbon-based photothermal materials and devices were employed for interfacial photothermal evaporation.[1,49–52]

In the present study, we have developed a facile cross-linking methodology for the fabrication of a carbon dot-based multifunctional photothermal evaporator suitable for solar steam generation, desalination, and water decontamination by incorporating it into bacterial cellulose. Lignin derived carbon dots (N-LCDs) showing excellent broad-spectrum absorption have been utilized to form *c*-BC@N-LCD, by a simple one-pot hydrothermal method. Here, the reusability issue with carbon dots has also overcome by cross-linking them with bacterial cellulose. The *c*-BC@N-LCD shows phenomenal light absorption in the NIR range. This solar evaporator has shown an evaporation rate of 2.2 kg m^{-2} h^{-1} under 1 sun illumination with good reusability, and robustness even after multiple purification cycles. Additionally, we demonstrate a high-performance solar purification from various sources and desalination as well as water remediation through the removal of heavy metal ions, pharmaceuticals, and dyes. To the best of our knowledge this material has been the very first report on the fabrication of a potent all-in-one photothermal membrane out of sustainable precursors like lignin and BC. Thus, the multifunctional *c*-BC@N-LCD can have a wide range of applications, ranging from large-scale industrial platforms to portable water purifying appliances.

Results and discussion

N-LCDs were prepared by one-pot hydrothermal synthesis using lignin as a precursor for carbon (C) and ethylenediamine (EDA) as an N dopant (Scheme 1). Notably, a deep black-brown colour dispersion was obtained after the hydrothermal synthesis of N-LCDs with an intense green color fluorescence (FL) (Fig. S1a, ESI†). The morphology of the N-LCDs was studied using transmission electron microscopy (TEM). Fig. S1b(i) and (ii) (ESI†) shows the presence of a homogenous distribution of spherical-shaped CDs throughout the solution. Notably the HR-TEM image of the N-LCDs shows a well-defined lattice fringe with a *d*-spacing of 0.24 nm that corresponds to the (112) plane

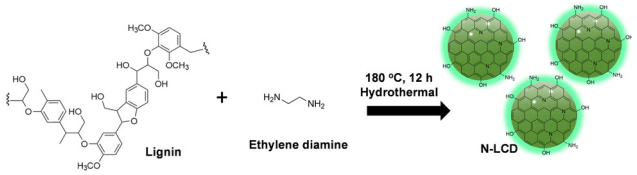

Scheme 1 Illustration of the synthesis of N-LCDs.

Published on 01 August 2024. Downloaded on 9/9/2025 11:02:34 PM.

of the graphitic structure (Fig. S1biii, ESI†). Fig. S1c (ESI†) reveals the histogram with the size distribution of the CDs falling in 2.4–4.2 nm range. A broad absorption spectrum of N-LCDs in Fig. S1d (ESI†) with peaks positioned at 290 nm belongs to π–π* transition occurring from core states of carbon and the peaks at 350 nm and 415 nm are obtained from n–π* transition from surface states.[53] The N-LCDs in solution yielded FL at 390 nm emissions with excitation wavelength of 410 nm due to the up-conversion FL phenomenon as indicated in Fig. S1e (ESI†). The yield of N-LCDs was found to be 619 mg mL^{-1}. This result demonstrates the potential of the as-prepared N-LCDs for sensing and photocatalytic applications. A broad diffraction peak in Fig. S1f (ESI†) is observed at 23.0° corresponding to the (002) plane of graphite.[54] The suitability of N-LCDs was checked by acquiring diffused reflectance spectra (DRS) of dried N-LCDs samples in the NIR range (700–2500 nm). As anticipated in Fig. S1g (ESI†), N-LCDs show very little reflectance loss, *i.e.*, 10.53%, making them an attractive photothermal substance for designing a robust interfacial solar evaporation platform. Furthermore, details of FTIR and XPS are given in the ESI† (Fig. S2).

Despite promising broadband absorption of N-LCDs, its photothermal activity can be exploited for solar evaporation applications only if it is stabilized against leaching to feed water media. This is because the size of photothermally active N-LCDs is in the 2.4–4.2 nm range. Here, we chose BC as a convenient porous and biocompatible substrate to accommodate N-LCDs without losing their photothermal activity. BC also serves as a superior thermal insulating platform, which would facilitate the effective thermal management in anticipated solar evaporating membranes during the interfacial evaporation process.[44] Detailed characterizations of BC are given in the ESI† (Fig. S3).

As a first trial, N-LCDs were incorporated into a BC matrix by an *in situ* hydrothermal method. BC@N-LCD obtained was black in colour and showed good NIR activity. However, we observed a decline of the solar evaporation efficiency upon repeated cycles. Therefore, we rationally designed a cross-linking strategy to covalently attach N-LCDs onto BC fibers. Incorporation of photothermally active N-LCDs in the BC matrix was carried out by preparing a homogenous solution of lignin and cross-linker epichlorohydrin (ECH), and afterward treating them hydrothermally. Scheme 2a illustrates the fabrication of a photothermally active evaporation membrane by direct incorporation of N-LCDs onto BC, while Scheme 2b illustrates the synthesis of *c*-BC@N-LCD by cross-linking N-LCDs onto BC. Furthermore, both the solar evaporation membranes were kept in water for 24 h under sunlight (Fig. S4, ESI†). In the former case (Fig. S4a, ESI†), the feed water evidently showed brown coloration due to slow leaching of N-LCDs from BC@N-LCD, showing the ineffectuality of appending N-LCDs to the BC matrix, whereas after cross-linking with ECH, *c*-BC@N-LCD (Fig. S4b, ESI†) imparted no visible coloration to feed water, showing the effective covalent anchoring of N-LCDs onto the BC fibrils.

The physical appearance of the as-synthesized *c*-BC@N-LCD hydrogel membrane is shown in Fig. 1a. The micromorphological characteristics of the *c*-BC@N-LCD composite were examined using TEM (Fig. 1b) and SEM (Fig. 1c), confirming that the N-LCDs are well bound to BC nanofibrils (see red arrows marked in Fig. 1b). A comparison of the FTIR curves obtained for *c*-BC@N-LCD with that of the non-crosslinked composite and N-LCDs are presented in Fig. 1d. A group of strong vibrations that emerged at 1005 cm^{-1}, 1028 cm^{-1}, and 1150 cm^{-1}, which are not much evident in the non-crosslinked BC@N-LCD composite, are attributed to C–O–C bonds formed *via* cross-linking with ECH. Peaks at 1640 cm^{-1} and 1430 cm^{-1} were attributed to C═O (carbonyl) stretching and C═C stretching (from aromatic rings) from the lignin moiety. The stretching vibrational peaks corresponding to C–H and O–H/N–H bonds are merged and appeared as a considerably broadband between 2700–3600 cm^{-1} in both N-LCDs and non-cross-linked BC@N-LCD. However, it is worth mentioning that the intensity of the O–H/N–H stretch vibrations (broad peak > 3000 cm^{-1}) is greatly reduced in *c*-BC@N-LCD because a large proportion of –OH and –NH moieties from N-LCDs were engaged in cross-linking by ECH. Furthermore, details of XPS are given in the ESI† (Fig. S5). Based on the above discussion, a plausible cross-linking mechanism is proposed and illustrated in Fig. 1e. In the presence of OH– in the reaction medium, alkoxide (–RO–) groups from BC and/or $–NH_2$ groups from N-LCDs can possibly react with ECH in two ways: one way is to form oxirane moieties in close vicinity by eliminating Cl^- (Fig. 1e(i) and (iii)), whereas a second possibility is to initiate oxirane ring opening as shown in Fig. 1e(ii).[55] It is worth mentioning that cross-linking might be possible with two N-LCDs and two cellulose nanofibers as well as between N-LCDs and BC. A representative cross-linked product is hence presented in Fig. 1e(iv) as a possible chemical structure of *c*-BC@N-LCD. Moreover, BET surface area analysis was performed to reveal the surface area and nature of porosity of the *c*-BC@N-LCD aerogel compared to the native BC material and details are given in the ESI† (Fig. S6). Besides, experiment details to prove the hydrophilicity and sorption capacity of *c*-BC@N-LCD by sessile drop contact angle tests were performed and given in the ESI† (Fig. S7).

The above design thus can greatly facilitate the interfacial heating since a better light-to-heat conversion for steam generation can be anticipated by using the 3D interconnected porous network of BC for hosting wide-spectrum active N-LCDs.[56] Furthermore, to evaluate the light harvesting capability of the *c*-BC@N-LCD hydrogel, we acquired its DRS spectrum in wet conditions (Fig. 2a). The percentage NIR reflectance

 This journal is © The Royal Society of Chemistry 2024

Published on 01 August 2024. Downloaded on 9/9/2025 11:02:34 PM.

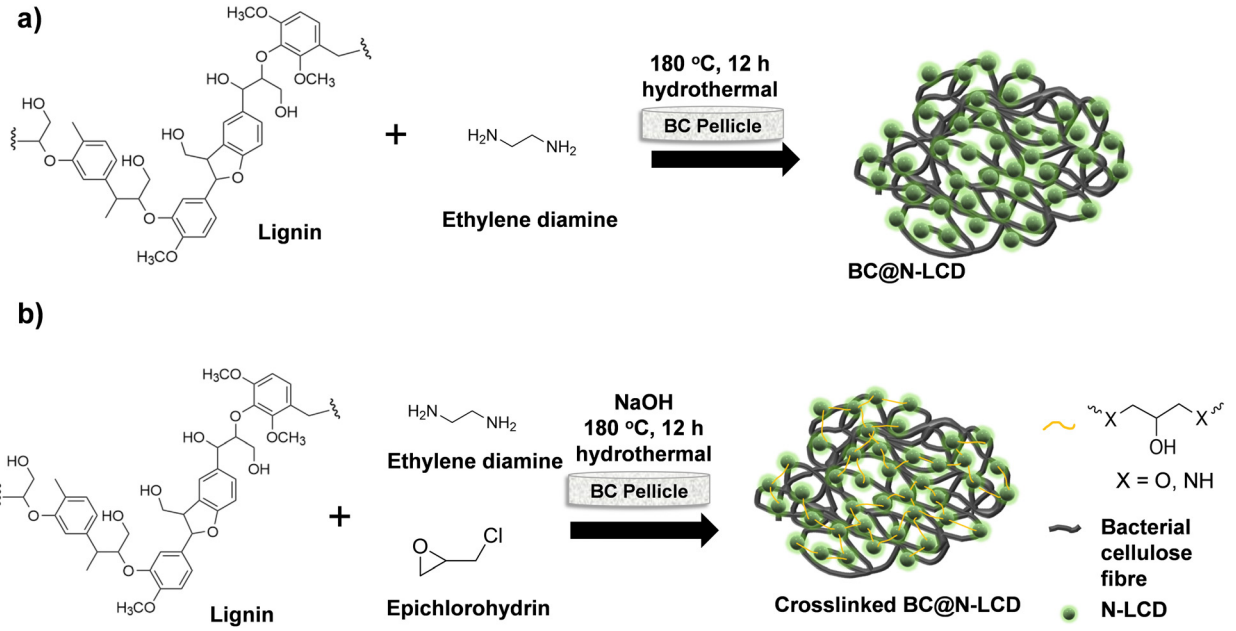

Scheme 2 Schematic illustration of: (a) synthesis of BC@N-LCD by direct incorporation of N-LCDs onto BC, and (b) synthesis scheme of *c*-BC@N-LCD by *in situ* cross-linking N-LCDs and BC.

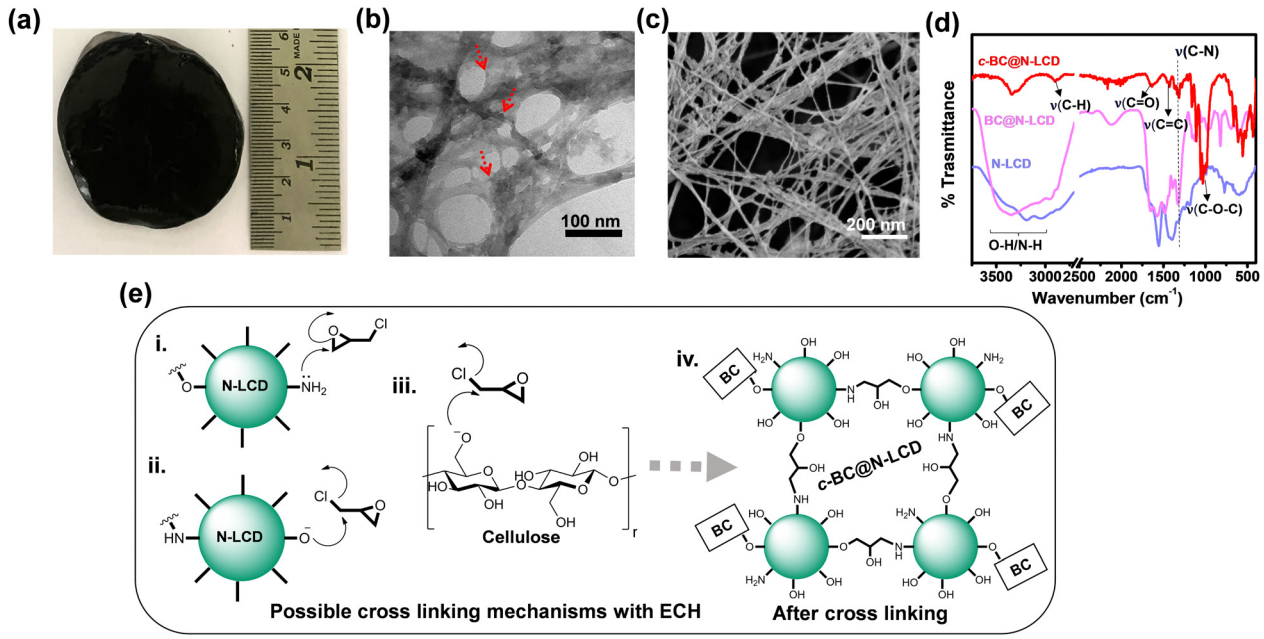

Fig. 1 (a) Digital photograph of the fabricated *c*-BC@N-LCD hydrogel. Morphological characterizations of *c*-BC@N-LCD by: (b) TEM (red dotted arrows point to the attached N-LCDs on BC fibres) and (c) SEM. Comparison study of *c*-BC@N-LCD, BC@N-LCD, and N-LCDs by (d) FTIR. (e) Possible mechanisms of cross-linking by ECH; (i) and (ii) linking with the oxirane moiety by eliminating Cl– of ECH by RO– from L-NCDs and BC, respectively, and (iii) opening of the oxirane ring by $-NH_2$ of L-NCDs. (iv) Representative structure of *c*-BC@N-LCD formed after cross-linking.

spectrum derived from DRS data is presented in Fig. 2b. NIR absorption of *c*-BC@N-LCD is calculated to be 88.1%. Furthermore, to verify the effective photothermal conversion by the composite, the temperature rise of *c*-BC@N-LCD was recorded while illuminating with 1 kW m^{-2} solar light. A temperature *vs.* time plot is drawn for the photothermal platform fabricated (Fig. 2c). A control BC and water is also kept for reference. In reconciliation with the above findings, the *c*-BC@N-LCD hydrogel is endowed with a captivating photothermal property and showed a sharp increase in surface temperature within the first

Published on 01 August 2024. Downloaded on 9/9/2025 11:02:34 PM.

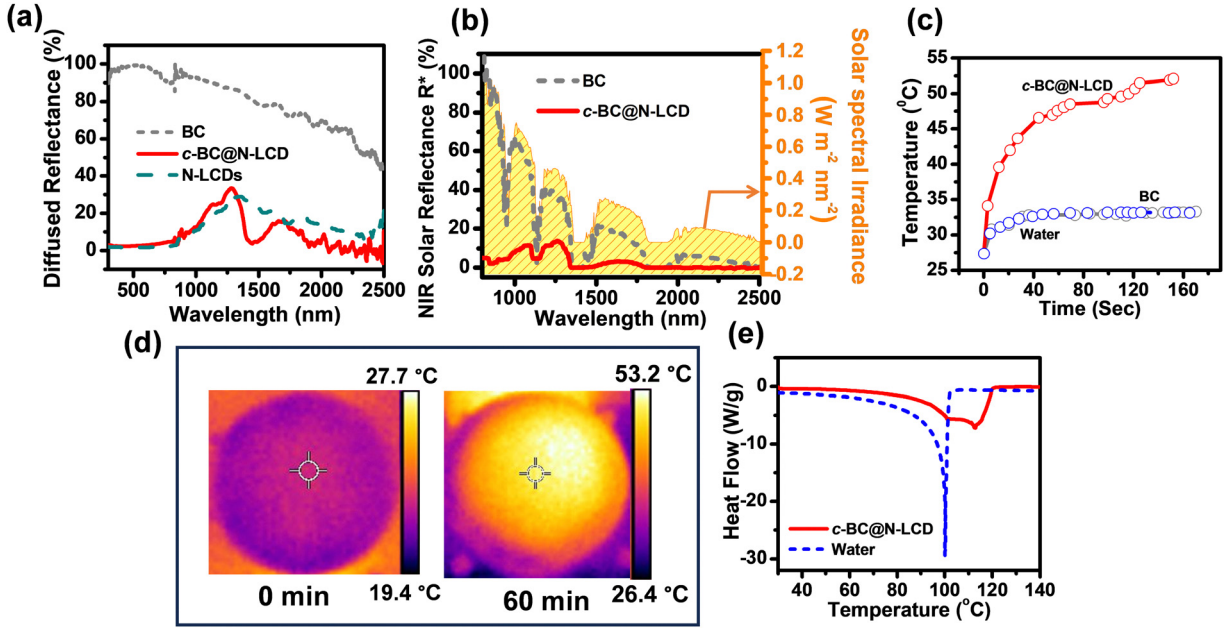

Fig. 2 (a) DRS of N-LCDs, BC and *c*-BC@N-LCD acquired in the full spectrum range and (b) corresponding % NIR reflectance. (c) The comparative temperature rise in water (blue), BC (grey) and *c*-BC@N-LCD (red) after illuminating the evaporator for approximately 2 min. (d) IR thermal image of BC and *c*-BC@N-LCD captured after illumination of 1 kW m^{-2} simulated solar light for 60 min (top view). (e) DSC curves showing a difference in evaporation of *c*-BC@N-LCD and pure water.

30 s and reached a highest temperature of 53.2 °C within 152 s upon illumination of 1 kW m^{-2} sunlight. Thermal profiles of the same composite captured by an infrared (IR) thermal imaging camera before and after illumination under 1 kW m^{-2} sunlight for 60 min are presented in Fig. 2d. The surface temperature of BC got increased only to some extent from 25.4 °C to 33.3 °C, whereas a visible surface temperature rise to 53.2 °C was noticed in *c*-BC@N-LCD. The effect of *c*-BC@N-LCD–water interaction on the overall evaporation performance of *c*-BC@N-LCD is a decisive factor to determine the total evaporation performance. The evaporation enthalpies (h_{LV}) of water alone and with *c*-BC@N-LCD were measured using a DSC experiment; thermograms are shown in Fig. 2e. A significant broadness in the evaporation peak of *c*-BC@N-LCD hydrogel can be seen in contrast to the sharp peak for pure water. Knowingly, liquid-to-gas transition happened sharply at boiling temperature in the case of free-state water and decreased immediately. However, evaporation started with less required energy in the hydrogel system and decreased gradually after reaching a maximum. It is remarkable that the completion of evaporation still happens at a higher temperature due to the considerable high energy needed for the evaporation of bound water. Additionally, the broadness of the evaporation curve indicates the existence of multiple possible water states due to the interaction between the cellulose polymer and water.[44] On the other hand, the overall h_{LV} of water from *c*-BC@N-LCD hydrogel was calculated to be 1971 kJ kg^{-1}, which is lower than the free water evaporation enthalpy, *i.e.*, 2267 kJ kg^{-1} (*i.e.*, close to theoretical value = 2260 kJ kg^{-1}). The substantial effective localization of heat generated at the *c*-BC@N-LCD–water interface (composite kept on the top of water which is taken in a cuvette) while irradiating with simulated sunlight (1 kW m^{-2}) is shown in the photographs of Fig. 3a (digital) and Fig. 3b (thermal). Once the practicality of *c*-BC@N-LCD as a photothermal platform for freshwater production was established, interfacial solar-driven evaporation experiments were accomplished using a lab-made setup in schematic Fig. 3c. In the next step, the evaporation performance of *c*-BC@N-LCD was correlated with two control experiments, *i.e.*, a pristine BC and the same volume of blank water. Cumulative water evaporation was observed in each case as plotted in Fig. 3d. *c*-BC@N-LCD hydrogel achieved an elevated ER, 2.2 kg m^{-2} h^{-1} and photothermal evaporation efficiency of 120.4% at solar irradiation of 1 kW m^{-2} verifying its excellent light-to-vapor conversion efficiency. The efficiency of above 100% can possibly come from the underestimation of the harvested solar energy, which is ultimately reflected in the final efficiency value. Also, several factors can lead to this speculation, such as (1) additional energy can be gained from the environment and (2) many factors such as uneven interfacial temperature across the membranes, and change in humidity can also lead to underestimation of light energy falling on the evaporator surface, *etc.*[57–59] Fig. 3e represents the comparative rate of water evaporated in BC, water, and *c*-BC@N-LCD. Table S1 (ESI†) tabulates the ERs obtained by the mass loss of water for *c*-BC@N-LCD, BC and blank water. In addition, the durability and stability of the *c*-BC@N-LCD hydrogel were tested for practical applications. After 10 cycles, the ER remains at 2.2 kg m^{-2} h^{-1} (Fig. 3f), indicating the longevity of the *c*-BC@N-LCD evaporator. Moreover, the effect of loading (Fig. S8) and variation in intensity of irradiation (Fig. S9) has been studied in detail and given in the ESI.† The evaporation performance of the as-fabricated

 This journal is © The Royal Society of Chemistry 2024

Published on 01 August 2024. Downloaded on 9/9/2025 11:02:34 PM.

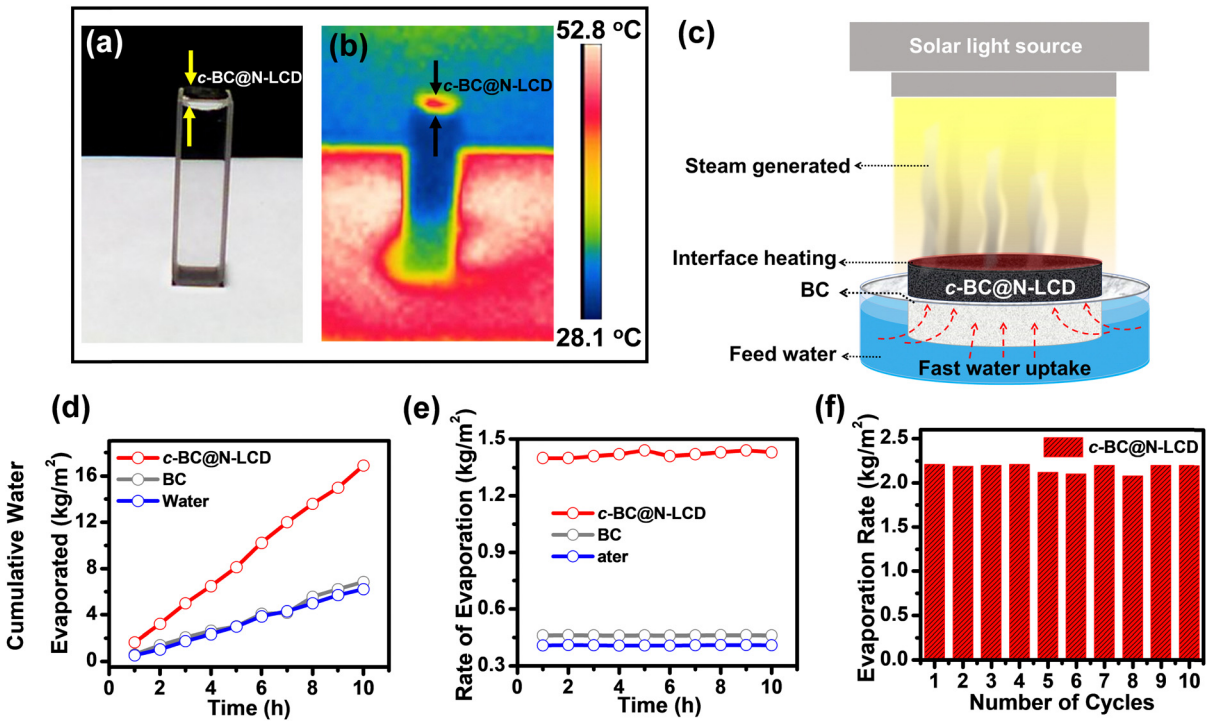

Fig. 3 (a) Digital and (b) IR thermal profile captured for demonstrating heat localization at the *c*-BC@N-LCD–water interface upon exposure to 1 kW m^{-2} solar light. (c) Schematic representation of a lab made setup used for solar evaporation experiments (red arrow marks signify effective up-side bulk water transportation). Comparative studies of water mass loss for BC, water, and *c*-BC@N-LCD; (d) cumulative mass of water evaporated *vs.* time plot, (e) rate performance plot, and (f) cyclic performance carried out for 10 cycles.

c-BC@N-LCD with several reported solar evaporators was compared and given in Table S2 (ESI†), indicating an excellent evaporation performance of our system achieved by following a simple fabrication strategy.

Moreover, for converting light energy into steam energy, ideal solar-driven water purifiers should be able to handle complex water sources, which often include pollutants like metal salts, organic compounds, and pharmaceuticals, *etc.* At first, the ERs of water from different water sources, including lake water, pond water, reverse osmosis water, tap water, river water, *etc.*, with *c*-BC@N-LCD were compared under real-time conditions (Fig. 4a, 21st November 2023, at 28 °C temperature, humidity = 56%). The ER using water from various sources as feed water under 1 kW m^{-2} sun irradiation in real time conditions was ~2.1–2.6 kg m^{-2} h^{-1}, which is higher than the rate obtained for ideal laboratory conditions. This might be due to wind (average 6 m s^{-1}) present in the outside atmosphere.

Furthermore, a conventional solar evaporator used for desalination accumulates the salt on the evaporator surface, obstructing the ability of evaporators to absorb sunlight and providing a passage for vapours to leave, which limits the vapour generation efficiency. Thus, a reliable solar desalination technique requires addressing the problems related with water fouling or salt accumulation. To quantitatively measure the water evaporation performance of *c*-BC@N-LCD in saline water, the mass change was measured by weighing balance *via* irradiating the *c*-BC@N-LCD under 1 kW m^{-2} sun power density. Fig. 4b indicates that the rate of evaporation under 1 sun illumination (1 kW m^{-2}) for saline water was measured to be 2.1 kg m^{-2} h^{-1} with evaporation efficiency up to 120% for five cycles (Fig. S10, ESI†). On the contrary, the evaporation rates of saline water with BC and with water were found to be 0.60 and 0.46 kg m^{-2} h^{-1}, respectively. The *c*-BC@N-LCD membrane retains its performance even after five cycles with saline solution, making it a suitable candidate for desalination.

Next, to prove the resilience of *c*-BC@N-LCD for the evaporation of polluted water, different simulated water feed was investigated. A major share of water pollution happened by indiscriminate release of pollutants like dyes, pharmaceuticals, metal salts, *etc.* from various industries. These toxic effluents contain unreacted chemicals and their by-products, which endanger aquatic as well as terrestrial life. As a concept model, the removal of various water polluting metal ions, dyes and a few pharmaceutical drugs using *c*-BC@N-LCD (3 × 3 cm^2) was tested with the corresponding simulated water samples and the results are presented in Fig. 4c–e. Efficient removal of metal ions like Cd^{2+}, Fe^{2+}, Ag^{+}, and Co^{2+}, from feed water by *c*-BC@N-LCD hydrogel within 2 h was observed (Fig. 4c). Removal of these metal ions was noticed both in light and dark conditions, with further details on the removal efficiency of metal ions given in the ESI,† which suggests that the metal ions probably get trapped by the surface amino and hydroxyl groups of N-LCDs, which are present even after cross-linking. Similarly,

Published on 01 August 2024. Downloaded on 9/9/2025 11:02:34 PM.

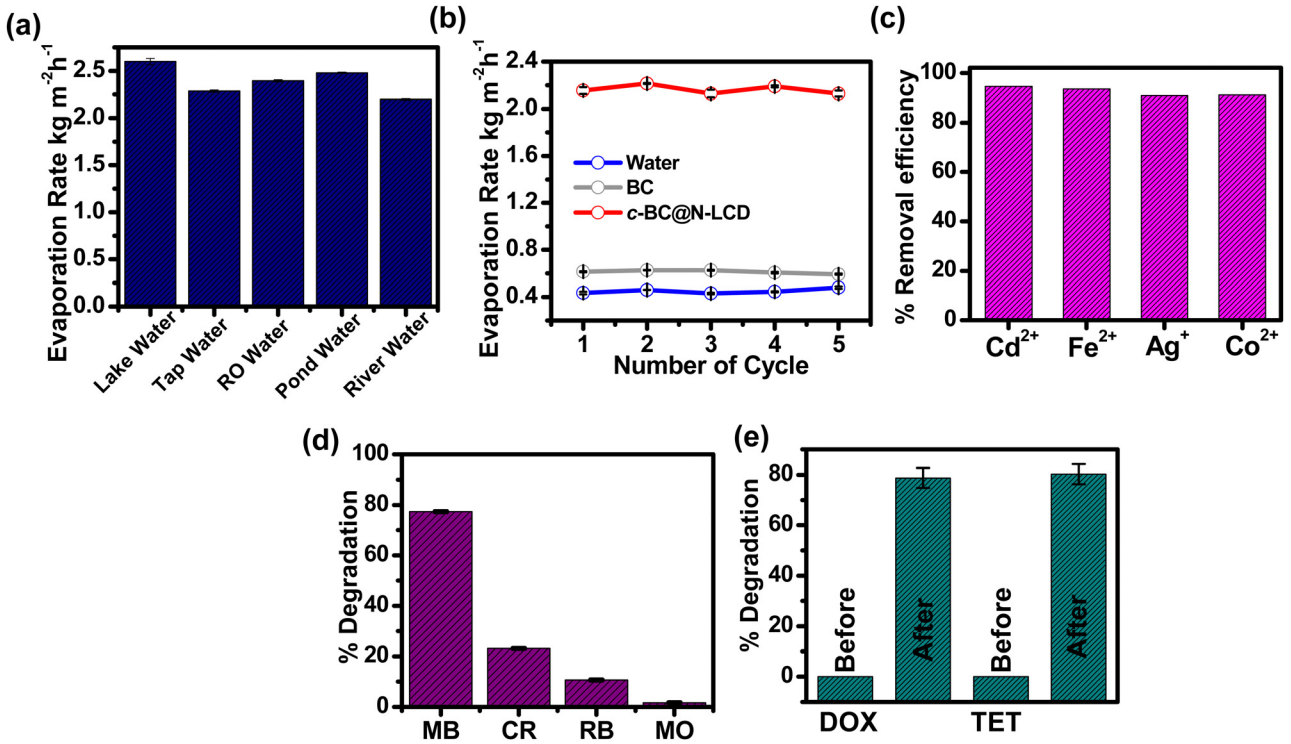

Fig. 4 Remediation of water by *c*-BC@N-LCD photothermal hydrogel membrane. Bar plots for: (a) evaporation rates calculated for various water sources, (b) rate of evaporation in saline water, (c) heavy metal ion removal from water bodies, (d) percentage degradation of various dyes from water bodies, and (e) percentage degradation of pharmaceutical drugs present in water. Samples were irradiated for 60 min with 1 kW m^{-2} solar light.

the degradation of dyes like methyl orange (MO), methylene blue (MB), rhodamine B (RB) and Congo red (CR) was analysed by means of UV-visible spectroscopy. Among them, MB shows a reduction in concentration after performing the degradation with *c*-BC@N-LCD hydrogel (irradiating under sunlight) shown in Fig. 4d. Fig. S11a (ESI†) presents the UV-visible absorption of MB dye simulated feed water before and after irradiation. The absorbance peak of MB almost disappeared after illuminating under sunlight for 60 min, indicating an efficient degradation of this cationic dye by N-LCDs, which are present in as-fabricated photothermal membrane. The degradation of MO has also been provided in Fig. S11b (ESI†), indicating that there has been no effect of N-LCDs on the degradation of MO after illumination, indicating selectivedegradation of MB among other dyes and details on selective degradation of MB are given in the ESI.† Finally, the potential of this photothermal platform for remediating pharmaceutical pollutants present in feed water was also tested with doxycycline (DOX) and tetracycline (TET) as model drugs. Initially, the characteristic peaks for DOX and TET were observed at 372 nm and 360 nm, respectively. After exposure to sunlight for 60 min, the peak intensity gets decreased, indicating a decrease in concentration of the pharmaceutical in the feed water. A bar diagram for % degradation before and after treatment with *c*-BC@N-LCD is provided in Fig. 4e indicating the excellent efficiency of this photothermal membrane towards environmental remediation. Besides, a real time outdoor experiment for freshwater collection has also been performed and details are given in the ESI† (Fig. S12).

Conclusions

A multifunctional *c*-BC@N-LCD hydrogel was fabricated from lignin-derived CDs cross-linked with BC. N-LCDs being a NIR active material, helped to harvest solar light and transform it to heat. The highly porous nature of BC, by virtue of the nanofibrous network structure, has high water uptake and serves as a support matrix for N-LCDs. The cross-linking between N-LCDs and BC by ECH has an important role toward stabilizing the membrane against leaching of photothermally-active N-LCDs. The as-fabricated solar water evaporator was demonstrated for generating clean water vapours and for decontaminating polluted water. The evaporator acquires high ER of 2.2 kg m^{-2} h^{-1}. Additionally, the versatility of as-developed evaporator was also checked with different water sources including saline water. The rate of evaporation during desalination was found to be ~2.1 kg m^{-2} h^{-1}. Besides, decontamination of water simulated with different classes of water pollutants (metal ion, dye, pharmaceutical drugs, *etc.*) was also successfully demonstrated. The as-designed *c*-BC@N-LCD, made from affordable, biocompatible, and ecofriendly building blocks, can therefore fit for purifying broad classes of water feeds.

Author contributions

The manuscript was written through contributions of all authors. All authors have given approval for the final version of the manuscript.

 This journal is © The Royal Society of Chemistry 2024

Published on 01 August 2024. Downloaded on 9/9/2025 11:02:34 PM.

Data availability

The data supporting this article have been included as part of the ESI.†

Conflicts of interest

There are no conflicts to declare.

Acknowledgements

S. M. M. gratefully acknowledges SP for his help in extending the characterization facilities at CSIR-NIIST. N. M. would like to thank UGC, New Delhi, for the research fellowship. K. N. thanks DBT-RA programme in Biotechnology and Life Sciences (DBTHRDPMU/DBT-RA/2022-23/EXT/59). S. M. M. thanks SERB-DST (CRG/2020/001769), BRNS (Project no. 58/14/17/2020-BRNS/37215), NTTM, Ministry of Textile, New Delhi, India and IIT Indore for financial support. The authors S. P. and G. P. acknowledge the CSIR's Fast Track Translation (FTT) project (MLP0077) for financial support. The authors gratefully acknowledge Sophisticated Instrumentation Centre (SIC), IIT Indore as well as AcSIR-NIIST for all the characterizations facilities.

Notes and references

1 N. Xu, J. Li, Y. Wang, C. Fang, X. Li, Y. Wang, L. Zhou, B. Zhu, Z. Wu, S. Zhu and J. Zhu, *Sci. Adv.*, 2019, **5**, eaaw7013.
2 H. Liang, Y. Mu, M. Yin, P.-P. He and W. Guo, *Sci. Adv.*, 2023, **9**, eadj1677.
3 F. Meng, Z. Ding, Z. Chen, K. Wang, X. Liu, J. Li, T. Lu, X. Xu and L. Pan, *J. Mater. Chem. A*, 2022, **10**, 9575–9581.
4 Z. Xu, J. Yu, H. Shan, J. Wang, J. Gao, Z. Ye and R. Wang, *Energy Environ. Sci.*, 2023, **16**, 5325–5338.
5 R. Zhu, M. Liu, Y. Hou, L. Zhang, M. Li, D. Wang, D. Wang and S. Fu, *ACS Appl. Mater. Interfaces*, 2020, **12**, 50113–50125.
6 P. R. Sharma, S. K. Sharma, T. Lindström and B. S. Hsiao, *Adv. Sustainable Syst.*, 2020, **4**, 1900114.
7 P. Cheng and D. Wang, *ACS Appl. Mater. Interfaces*, 2023, **15**, 8761–8769.
8 Y. Guo, X. Zhao, F. Zhao, Z. Jiao, X. Zhou and G. Yu, *Energy Environ. Sci.*, 2020, **13**, 2087–2095.
9 Y. Kuang, C. Chen, S. He, E. M. Hitz, Y. Wang, W. Gan, R. Mi and L. Hu, *Adv. Mater.*, 2019, **31**, 1900498.
10 Y. Bu, Y. Zhou, W. Lei, L. Ren, J. Xiao, H. Yang, W. Xu and J. Li, *J. Mater. Chem. A*, 2022, **10**, 2856–2866.
11 R. Niu, Y. Ding, L. Hao, J. Ren, J. Gong and J. Qu, *ACS Appl. Mater. Interfaces*, 2022, **14**, 45533–45544.
12 Y. Fan, Z. Tian, F. Wang, J. He, X. Ye, Z. Zhu, H. Sun, W. Liang and A. Li, *ACS Appl. Energy Mater.*, 2021, **4**, 2932–2943.
13 L. Gong, J. Sun, P. Zheng, F. Lin, G. Yang and Y. Liu, *ACS Appl. Mater. Interfaces*, 2021, **13**, 17649–17657.
14 D. Zhang, Y. Cai, Q. Liang, Z. Wu, N. Sheng, M. Zhang, B. Wang and S. Chen, *ACS Sustainable Chem. Eng.*, 2020, **8**, 9017–9026.
15 Z.-C. Xiong, Y.-J. Zhu, D.-D. Qin and R.-L. Yang, *ACS Appl. Mater. Interfaces*, 2020, **12**, 32556–32565.
16 D. P. Storer, J. L. Phelps, X. Wu, G. Owens, N. I. Khan and H. Xu, *ACS Appl. Mater. Interfaces*, 2020, **12**, 15279–15287.
17 T.-H. Huang, X.-Y. Tian, Y.-Y. Chen, J. Widakdo, H. F. M. Austria, O. Setiawan, T. M. Subrahmanya, W.-S. Hung, D.-M. Wang, C.-Y. Chang, C.-F. Wang, C.-C. Hu, C.-H. Lin, Y.-L. Lai, K.-R. Lee and J.-Y. Lai, *Adv. Funct. Mater.*, 2024, **34**, 2308321.
18 Y. Jin, X. Gong, Y. He, H. Wang, S. Li and J. Liu, *Solar RRL*, 2023, **7**, 2300548.
19 Z.-C. Xiong, Y.-J. Zhu, D.-D. Qin, F.-F. Chen and R.-L. Yang, *Small*, 2018, **14**, 1803387.
20 M. U. Farid, J. A. Kharraz and A. K. An, *ACS Appl. Mater. Interfaces*, 2021, **13**, 3805–3815.
21 S.-Q. Li, Y. Deng, J. Huang, P. Wang, G. Liu and H.-L. Xie, *Aggregate*, 2023, **4**, e371.
22 S. Chhetri, A. T. Nguyen, S. Song, D. H. Park, T. Ma, N. Gaillard, S.-H. Yoon and W. Lee, *ACS Appl. Mater. Interfaces*, 2023, **15**, 54773–54785.
23 H. Liu, F. Wu, X.-Y. Liu, J. Yu, Y.-T. Liu and B. Ding, *Nano Lett.*, 2023, **23**, 11907–11915.
24 Y. Qian, G. Xue, L. Chen, G. Xu and G.-E. Wang, *Adv. Mater.*, 2024, **36**, 2310795.
25 L. Wang, W. Li, L. Yin, Y. Liu, H. Guo, J. Lai, Y. Han, G. Li, M. Li, J. Zhang, R. Vajtai, P. M. Ajayan and M. Wu, *Sci. Adv.*, 2020, **6**, eabb6772.
26 I. Rahmawati, Indriyati, F. A. Permatasari, M. A. Irham, M. I. Nugraha, T. D. Anthopoulos and F. Iskandar, *ACS Appl. Nano Mater.*, 2023, **6**, 2517–2526.
27 N. Mate, D. Khandelwal, K. Nabeela and S. M. Mobin, *J. Mater. Chem. C*, 2023, **11**, 16201–16213.
28 T. C. Wareing, P. Gentile and A. N. Phan, *ACS Nano*, 2021, **15**, 15471–15501.
29 J. Gan, L. Chen, Z. Chen, J. Zhang, W. Yu, C. Huang, Y. Wu and K. Zhang, *Small*, 2023, **19**, 2304066.
30 M. Lawoko, L. Berglund and M. Johansson, *ACS Sustainable Chem. Eng.*, 2021, **9**, 5481–5485.
31 A. A. Dar, M. Usman, W. Zhang, Q. Zhu, B. Pan, A. Sial and C. Wang, *ACS ES&T Eng.*, 2022, **2**, 1942–1952.
32 N. Mate, Pranav, K. Nabeela, N. Kaur and S. M. Mobin, *ACS Omega*, 2022, **7**, 43759–43769.
33 W. Chao, Y. Li, X. Sun, G. Cao, C. Wang and S.-H. Ho, *Chem. Eng. J.*, 2021, **405**, 126703.
34 S. K. Bhattacharyya, M. Dule, R. Paul, J. Dash, M. Anas, T. K. Mandal, P. Das, N. C. Das and S. Banerjee, *ACS Biomater. Sci. Eng.*, 2020, **6**, 5662–5674.
35 M. Zhang, J. Xue, Y. Zhu, C. Yao and D. Yang, *ACS Appl. Mater. Interfaces*, 2020, **12**, 22191–22199.
36 J. Huang, X. Liu, L. Li, S. Chen, J. Yang, J. Yan, F. Xu and X. Zhang, *ACS Sustainable Chem. Eng.*, 2021, **9**, 15190–15201.
37 J.-S. Wei, T.-B. Song, P. Zhang, Z.-Y. Zhu, X.-Y. Dong, X.-Q. Niu and H.-M. Xiong, *ACS Appl. Energy Mater.*, 2020, **3**, 6907–6914.

Published on 01 August 2024. Downloaded on 9/9/2025 11:02:34 PM.

38 A. Dong, W. Xiao, W. Yuan and K. Zuo, *ACS Appl. Polym. Mater.*, 2023, **5**, 9564–9573.
39 Z. Li, Y. Zhang, Q. Huang, Z. Chen, W. Wang and W. Li, *ACS Appl. Mater. Interfaces*, 2023, **15**, 11827–11836.
40 H. M. Wilson, H. W. Lim and S. J. Lee, *ACS Appl. Mater. Interfaces*, 2022, **14**, 47800–47809.
41 Y. Lu, D. Fan, Y. Wang, H. Xu, C. Lu and X. Yang, *ACS Nano*, 2021, **15**, 10366–10376.
42 P. V. Devre and A. H. Gore, *Langmuir*, 2024, **40**, 141–158.
43 L. Jiao, W. Xu, H. Yan, Y. Wu, W. Gu, H. Li, D. Du, Y. Lin and C. Zhu, *Chem. Commun.*, 2019, **55**, 9865–9868.
44 K. Nabeela, M. N. Thorat, S. N. Backer, A. M. Ramachandran, R. T. Thomas, G. Preethikumar, A. P. Mohamed, A. Asok, S. G. Dastager and S. Pillai, *ACS Appl. Bio Mater.*, 2021, **4**, 4373–4383.
45 M. Jin, Z. Wu, F. Guan, D. Zhang, B. Wang, N. Sheng, X. Qu, L. Deng, S. Chen, Y. Chen and H. Wang, *ACS Appl. Mater. Interfaces*, 2022, **14**, 12284–12294.
46 Q. Jiang, H. G. Derami, D. Ghim, S. Cao, Y.-S. Jun and S. Singamaneni, *J. Mater. Chem. A*, 2017, **5**, 18397–18402.
47 N. Li, L. Qiao, J. He, S. Wang, L. Yu, P. Murto, X. Li and X. Xu, *Adv. Funct. Mater.*, 2021, **31**, 2008681.
48 X. Song, W. Dong, Y. Zhang, H. M. Abdel-Ghafar, A. Toghan and H. Jiang, *Exploration*, 2022, **2**, 20220054.
49 D.-D. Qin, Y.-J. Zhu, F.-F. Chen, R.-L. Yang and Z.-C. Xiong, *Carbon*, 2019, **150**, 233–243.
50 G. Wang, Y. Fu, A. Guo, T. Mei, J. Wang, J. Li and X. Wang, *Chem. Mater.*, 2017, **29**, 5629–5635.
51 H. Wang, A. Du, X. Ji, C. Zhang, B. Zhou, Z. Zhang and J. Shen, *ACS Appl. Mater. Interfaces*, 2019, **11**, 42057–42065.
52 Y. Li, Y. Shi, H. Wang, T. Liu, X. Zheng, S. Gao and J. Lu, *Carbon Energy*, 2023, **5**, e331.
53 N. Soni, S. Singh, S. Sharma, G. Batra, K. Kaushik, C. Rao, N. C. Verma, B. Mondal, A. Yadav and C. K. Nandi, *Chem. Sci.*, 2021, **12**, 3615–3626.
54 S. Burai, N. Ghorai, H. N. Ghosh and S. Mondal, *J. Phys. Chem. C*, 2022, **126**, 20092–20100.
55 S. Singh, N. Shauloff and R. Jelinek, *ACS Sustainable Chem. Eng.*, 2019, **7**, 13186–13194.
56 P. Tao, G. Ni, C. Song, W. Shang, J. Wu, J. Zhu, G. Chen and T. Deng, *Nat. Energy*, 2018, **3**, 1031–1041.
57 P. Yuan, C. Men, L. Zhao, P. Cao, Z. Yang, Y. Niu, Y. Zhang, Y. Yu and Q. Li, *ACS Appl. Mater. Interfaces*, 2022, **14**, 15549–15557.
58 Y. Wang, X. Wu, X. Yang, G. Owens and H. Xu, *Nano Energy*, 2020, **78**, 105269.
59 S. Hong, Y. Shi, R. Li, C. Zhang, Y. Jin and P. Wang, *ACS Appl. Mater. Interfaces*, 2018, **10**, 28517–28524.

 This journal is © The Royal Society of Chemistry 2024